Biosensors and Bioelectronics 188 (2021) 113337

Contents lists available at ScienceDirect

Biosensors and Bioelectronics

journal homepage: www.elsevier.com/locate/bios

A dual-model "on-super off" photoelectrochemical/ratiometric electrochemical biosensor for ultrasensitive and accurate detection of microRNA-224

Ruiying Yang [a], Guihua Jiang [b], Huimin Liu [a], Leiliang He [a], Fei Yu [a], Li'e Liu [a], Lingbo Qu [c], Yongjun Wu [a,b,*]

[a] College of Public Health, Zhengzhou University, Zhengzhou, 450001, China
[b] College of Chemistry, Zhengzhou University, Zhengzhou, 450001, China
[c] Institute of Green Catalysis, College of Chemistry, Zhengzhou University, Zhengzhou, 450001, China

ARTICLE INFO

Keywords:
Dual-model
Photoelectrochemical biosensor
Ratiometric electrochemical biosensor
MicroRNA-224
Signal amplification strategies

ABSTRACT

A dual-model "on-super off" photoelectrochemical (PEC)/ratiometric electrochemical (EC) biosensor based on signal enhancing and quenching combining three-dimensional (3D) DNA walker strategy was designed for the ultrasensitive and accurate detection of microRNA-224 (miRNA-224). The "signal on" PEC state was achieved by methylene blue labeled hairpin DNA (MB-DNA) for sensitizing CdS QDs. Then numerous transformational ferrocene labeled DNAs (Fc-DNAs) converted by target-induced 3D DNA walker amplification with the help of Ag nanocubes (NCs) label DNA (Ag-DNA) were introduced to open hairpin MB-DNA. Such configuration change would relocate the sensitizer MB and the quencher Fc, whereas energy transfer placed between Ag NCs and CdS QDs, thereby significantly quenching the PEC signal to obtain "super off" state. Meanwhile, these changes resulted in a decreased oxidation peak current of MB (I_{MB}) and an increased that of Fc (I_{Fc}). MiRNA-224 was also detected on basis of the dual-signaling EC ratiometric method for complementary PEC detection. Benefiting from different mechanisms and relatively independent signal transduction, this approach not only avoided interference from difficult assembly but also outstandingly increased sensitivity by distance-controllable signal enhancing and quenching strategies. As a result, the detection ranges of 0.1–1000 fM with a low detection limit of 0.019 fM for PEC, and 0.52 to 500 fM with a low detection limit of 0.061 fM for EC, were obtained for miRNA-224, which opens a new avenue for designing numerous elegant biosensors with potential utility in bioanalysis and early disease diagnosis.

1. Introduction

MicroRNAs (miRNAs) are a class of short, single-stranded, endogenous noncoding RNAs (ca. 18–25 nt) (Zhang et al., 2016, 2018a), which has been served as a promising biomarker candidates for cancer initiation and progression (Zhang et al., 2018b; Cao et al., 2018). However, because of their small size, ultra-low abundance, and sequence similarity, reliable and sensitive detection of miRNAs is still a rigorous challenging puzzle. Currently, many approaches have been reported for miRNAs assay, such as surface plasmon resonance (Gu et al., 2017), electrochemistry (Cheng et al., 2019; Zhang et al., 2017), fluorescence (Dong et al., 2018; Li et al., 2018), electrochemiluminescence (Gao et al., 2019; Ye et al., 2019). Even if these methods present many improvements, some disadvantages, such as miscellaneous equipment, large expense, and low sensitivity, have made disease diagnosis by miRNAs detection an enormous challenge. Therefore, it is vital to exploit highly sensitive, low cost, and accurate biosensing technique for miRNAs analysis.

Photoelectrochemical (PEC) biosensor, as a rapidly developed analytical technology in biomarker assay and early cancer diagnosis, possesses simple instrumentation, inexpensive, and highly sensitive, and has drawn wide research interest (Yang et al., 2018; Gao et al., 2020; Lv et al., 2020; Li et al., 2021). To date, various signal amplification strategies have been made on constructing PEC biosensors for miRNAs assay to achieve high detection sensitivity (Zhu et al., 2019; Li et al., 2020a,b), including sensitization strategies of photoactive materials (noble

* Corresponding author. College of Public Health, Zhengzhou University, Zhengzhou, 450001, China.
E-mail address: wuyongjun135@126.com (Y. Wu).

https://doi.org/10.1016/j.bios.2021.113337
Received 10 February 2021; Received in revised form 22 April 2021; Accepted 11 May 2021
Available online 14 May 2021

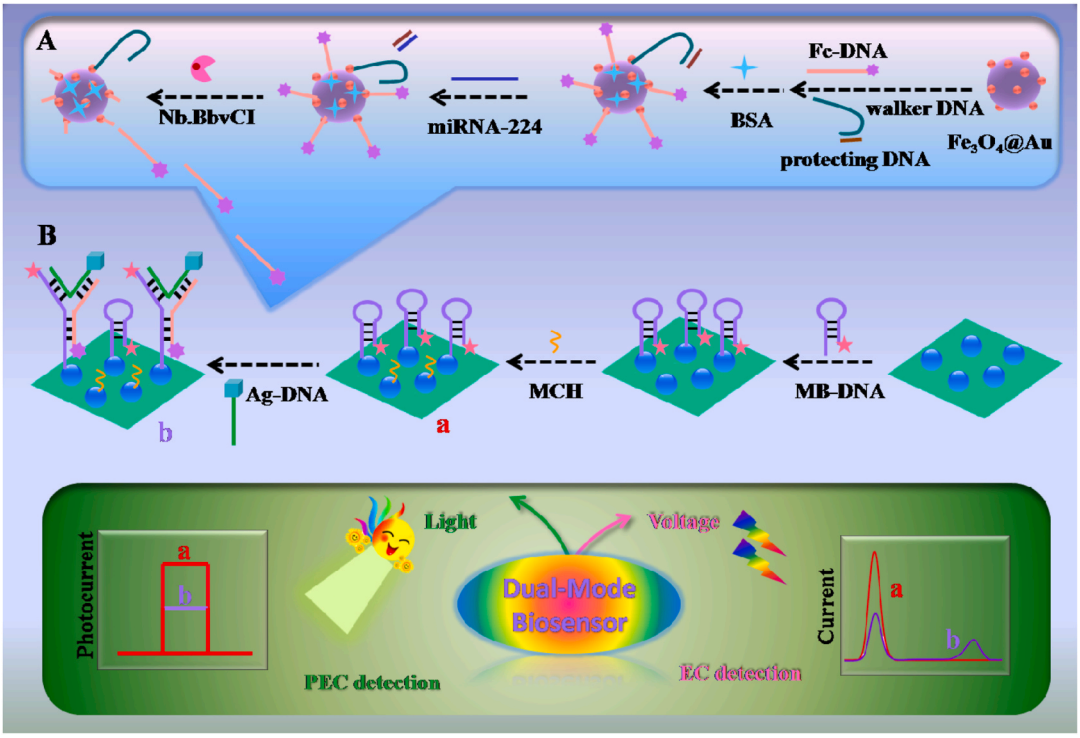

Scheme 1. Schematic diagram of the dual-model PEC and EC biosensor for miRNA-224 detection.

metal/dye-sensitized semiconductors, heterojunction semiconductors, etc.) and DNA amplification techniques of targets (such as DNA motor, DNA walker, etc.). For example, a PEC biosensor based on bipedal DNA walker-triggered signal quenching and enhancing was developed for miRNA-21 detection (Zhu et al., 2019). A novel PEC bioassay was achieved for miRNA-21 detection based on direct exciton−plasmon interactions between CdS QDs and noble metal nanoparticles (Ma et al., 2016). A triple-helix molecular switch PEC biosensor was reported for miRNA-141 assay combined with three-dimensional (3D) DNA walker-induced signal amplification (Yang et al., 2019b). Inspired by these works, an energy-transfer PEC biosensor based on methylene blue (MB)/ferrocene (Fc)-induced signal quenching and enhancing coupling 3D DNA walker signal amplification is highly promising for ultrasensitive detection of miRNAs.

Although the PEC biosensing platform possesses many merits, it still struggles to satisfy the increased analysis requirements of reliability and reproducibility if only the single-modality assay is employed. Thus, many research groups began to exploit the dual-model biosensors on account of different signal conversion modes and transmission mechanisms, whereas the two signal paths were relatively independent and allowed cross-check to each other (Deng et al., 2020; Kong et al., 2018; Ge et al., 2019). So, some interference errors caused by detection condition and personnel operation were corrected. Recently, the dual-signaling electrochemical (EC) ratiometric biosensor based on "signal-on" and "signal-off" strategies, has attracted growing attentions in DNA assay and protein detection, because of its excellent analysis capability, such as low background noise, wide linear range, low detection limit, good reliability and reproducibility (Zhu et al., 2018; Gai et al., 2017; Li et al., 2019a). For instance, a triple-helix molecular switch EC ratiometric sensor was reported for nucleic acids assay used MB and Fc as tags (Xiong et al., 2017). A bifunctional DNAzyme nanodevice-based ratiometric EC biosensor was constructed for sensitive and accurate mercury ion assay (Li et al., 2019b). This inspires us to construct a biofunctionalized nanostructures-driven dual-model PEC/ratiometric EC biosensor for miRNA-224 detection combining 3D DNA walker strategy.

Herein, a versatile dual-model "on−super off" PEC/ratiometric EC biosensor was developed for highly sensitive and reliable detection of miRNA-224 by coupling target-induced 3D DNA walker circular amplification strategy with the distance-controllable signal enhancing and quenching. As shown in Scheme 1A, a 3D DNA walker was developed for achieving the conversion and amplification of miRNA-224 through Fe_3O_4@Au nanoparticles as substrate to immobilize walker DNA and support DNA (Fc-DNA), where walker DNA paired with protecting DNA. In the presence of miRNA-224, walker DNA was released and then paired with Fc-DNA, resulting in the formation of recognition site for Nb.BbvCI nicking endonuclease. So, under the nicking of Nb.BbvCI, the intermediate Fc-DNA was generated along with the releasing of walker DNA which would match with another support DNA. In this way, lots of intermediate Fc-DNAs were achieved. As depicted in Scheme 1B, CdS QDs with impressive photoelectric conversion efficiency was employed as a photoactive electrode material. After immobilization of MB labeled hairpin DNA (MB-DNA) via Cd–S bonds (Yang et al., 2019b), an outstanding "signal on" state was achieved on account of the excellent sensitizing effect from MB toward CdS, leading to a desirable initial amplified PEC signal. Subsequently, transformational Fc-DNA and Ag nanocubes (NCs) labeled auxiliary probe DNA (Ag-DNA) were introduced to open the hairpin MB-DNA, resulting in the form of a "Y"-shaped junction structure via hybridization between DNA sequences. This configuration change would adjust the sensitizer MB away from of CdS QDs, make the Fc as a quencher close enough to CdS QDs, and place Ag NCs at the other terminal whereas energy transfer between Ag and CdS, thereby significantly quenching the PEC signal to obtain "super off" state. Dexterously, MB and Fc have excellent electrochemical activity and can produce obvious electrochemical signals. As a result, the oxidation peak current of MB (I_{MB}) was decreased and that of Fc (I_{Fc}) was increased. MiRNA-224 was detected on basis of the dual-signaling EC ratiometric method for complementary PEC detection. Benefiting from different mechanisms and relatively independent signal transduction, the interference between two signals in the dual-model biosensor can be effectively reduced, which opens a new avenue for designing numerous elegant biosensors with excellent property.

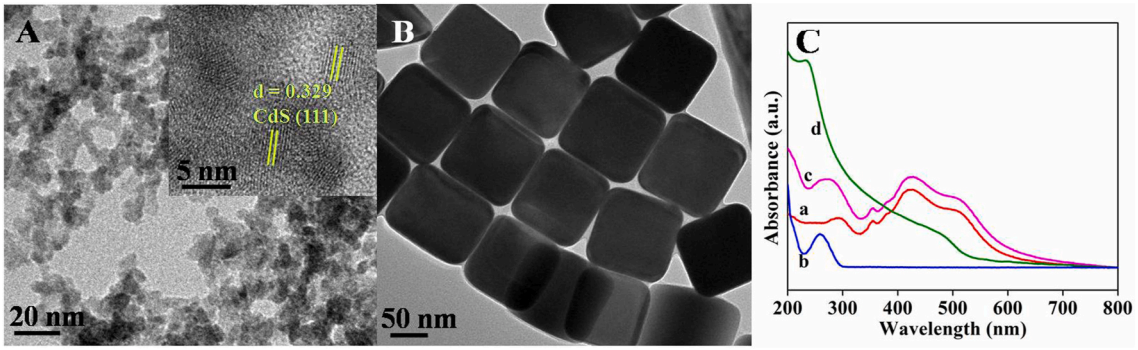

Fig. 1. TEM images of (A) CdS QDs (insert: HRTEM image of CdS QDs) and (B) Ag NCs, (C) UV–vis spectra of (a) Ag, (b) DNA, (c) Ag-DNA and (d) CdS QDs.

2. Experimental section

2.1. Preparation of Ag NCs and signal probe

The preparation of Ag NCs was similar to that before with slight modifications (Tao et al., 2006). Briefly, $CuCl_2$ (7 μL, 0.047 mol/L) was added into 2 mL of 1,5-pentanediol solution containing $AgNO_3$ (0.165 mol/L) as solution 1. PVP (40 mg) was dissolved into 2 mL of 1,5-pentanediol as solution 2. 1,5-pentanediol (5 mL) was heated to 190 °C at reflux for 2 min, to which was added alternately two precursor solutions at different rates: 125 μL of solution 1 every minute and 80 μL of solution 2 every 30 s. After repeating this addition for eight times, the reaction was continued for 2 min and quenched by transferring the solution into an ice-cold water bath. The product was collected by centrifugation and successively washed with acetone and water. The resulting Ag NCs were re-dispersed into 100 mL of water for further use. For the preparation of signal probe, 50 μL of 10 μM DNA were separately incubated with 1 mL of Ag NCs under gentle shaking for 12 h to achieve Ag-DNA.

2.2. Preparation of transformational Fc-DNAs

First, walker DNA (10 μM, 20 μL) and protecting DNA (10 μM, 40 μL) were heated at 95 °C for 5 min, and subsequently naturally cooled to form (double-stranded DNAs) dsDNAs (Zhu et al., 2019; Gao et al., 2019; Xu et al., 2019). Afterward, dsDNAs (20 μL) and support DNA (50 μM, 20 μL) were added in PBS (40 μL, 10 mM TCEP, pH 7.4) for 60 min to reduce disulfide bonds, followed by the addition of the Fe_3O_4@Au NPs (15 mg mL^{-1}, 20 μL, the synthesis and characterization of Fe_3O_4@Au NPs was provided in the Supporting Information). Then the mixture was slightly shaken for 16 h at 4 °C. Afterward, using BSA to block the nonspecific adsorption sites, the Fe_3O_4@Au-dsDNAs were achieved by magnetic separation and washing. When different-concentration miRNA-224 (50 μL) existed, walker DNA was released and then hybridized with support DNA for 1 h at 37 °C. After that, 10 U Nb.BbvCI was appended and maintained 2 h at 37 °C to nick the specific recognition site and generated transformational Fc-DNAs. At last, abundant transformational Fc-DNAs were achieved through magnetic separation.

2.3. Fabrication of the dual-model PEC and EC biosensor

Before use, ITO electrodes were sequentially ultrasonically treated with acetone, NaOH (1 M), and H_2O. Subsequently, 25 μL CdS QDs solution (the preparation of CdS QDs was provided in the Supporting Information) was drop-cast onto the surface of the cleaned ITO electrode and dried in air, labeled as ITO/CdS electrode. Prior to modification on the ITO/CdS electrode, MB-DNA was dissolved in 20 mM PBS (pH 7.4, 10 mM TCEP, 2.5 mM $MgCl_2$, 50 mM NaCl) under darkness for 1 h to eliminate disulfide bonds, then adding 20 μL of 1 μM MB-DNA onto the ITO/CdS electrode at 4 °C for 12 h. To block the nonspecific sites of ITO/CdS/MB-DNA electrode, 2 mM MCH was added and incubated for 1 h. Afterward, 20 μL solution containing Ag-DNA and the above intermediate Fc-DNA which linearly correlated with target miRNA-224, was dipped onto the resulting ITO/CdS/MB-DNA/MCH electrode for 2 h at 37 °C. Finally, PEC measurement of the designed biosensor was carried out in Tris–HCl solution (0.1 M, pH 7.4) containing AA (0.1 M) at 0 V, and the electrochemical capability of the resulting electrode was characterized using square wave voltammetry (SWV) with a step potential of 4 mV, a frequency of 25 Hz, and an amplitude of 25 mV in the potential range between −0.5 and 0.6 V.

3. Results and discussion

3.1. Materials characterization

The morphology and microstructure of the as-synthesized materials were surveyed by TEM and the high-resolution TEM (HRTEM). From Fig. 1A, CdS QDs exhibited an average sizes of 8 nm, and lattice fringes with a distance of 0.289 nm corresponding to the (200) crystalline plane of CdS (Yang et al., 2019a). The resulting Ag NCs had uniform morphologies with an average side length of ~100 nm (Fig. 1B), and characteristic absorption peaks (Fig. 1C, curve a) (Tao et al., 2006; Xue et al., 2018). After DNA sequence was modified onto the surface of Ag NCs, the curve c appeared a new absorbance peak at about 260 nm corresponding to the typical peak of oligonucleotides, demonstrating the successful preparation of Ag-DNA (Ma et al., 2016). Particularly, a large spectral overlap was observed between the plasmon band of Ag NCs and the absorption spectrum of the CdS QDs, which makes for occurring of efficient energy transfer (curve d).

3.2. The feasibility and signal amplification mechanism of dual-model biosensor

To confirm the feasibility of dual-model biosensor, the 3D DNA walker-induce the conversion and amplification of miRNA-224 were performed by 13% PAGE image. From Fig. S2, a single distinct band of walker DNA was observed (lane 1). As walker DNA firstly paired with protecting DNA, two separate bands could be seen (lane 3), where the top band was corresponded to the hybridized dsDNA of walker-protecting DNA, and the bottom band was Fc-DNA. In the presence of target miRNA-224, new separate bands appeared (lane 2). Because miRNA-224 was added to pair with protecting DNA (the top band) for releasing of walker DNA which further paired with Fc-DNA (the bottom band). Besides, the middle band was the remained walker DNA. Then 10 U Nb.BbvCI was added into the mixture of walker DNA and Fc-DNA, resulting in the appearance of new bands (lane 4). The band at the low position corresponded to the intermediate Fc-DNA released from the walker-support dsDNA. Besides, the band at the high position was similar to walker DNA, indicating the successful releasing of walker DNA. These results confirm the potential of 3D DNA walker for achieving the conversion and amplification of miRNA-224.

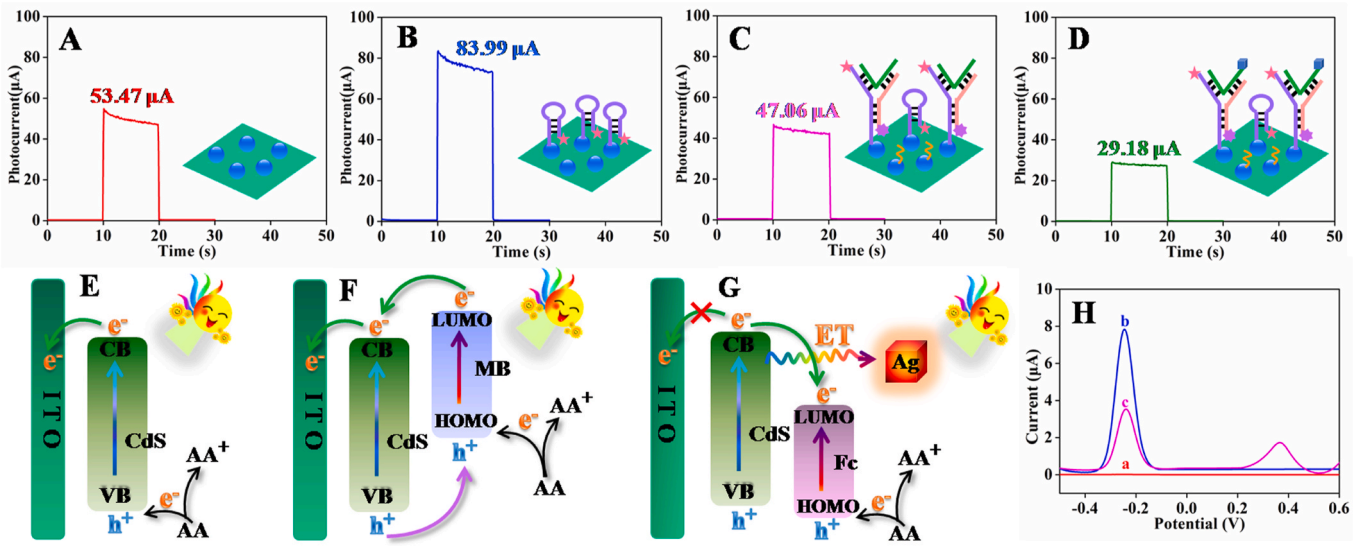

Fig. 2. Photocurrent signals of (A) ITO/CdS, (B) ITO/CdS/MB-DNA, (C) ITO/CdS/MB-DNA/MCH electrode after incubation with transformational Fc-DNA and DNA, and (D) ITO/CdS/MB-DNA/MCH electrode after incubation with transformational Fc-DNA and Ag-DNA. The possible photocurrent mechanism of (E) CdS, (F) CdS/MB and (G) CdS/Fc/Ag system. (H) EC responses of (a) ITO/CdS, (b) ITO/CdS/MB-DNA, and (c) ITO/CdS/MB-DNA/MCH after incubation with transformational Fc-DNA and Ag-DNA.

To explore the signal amplification mechanism of biosensor, the photocurrent of different assembled electrodes were characterized. As described in Fig. 2, the ITO/CdS electrode produced a suitable initial photocurrent of ~53.47 μA (Fig. 2A), whereas a photocurrent of ~83.99 μA appeared after the introduction of MB onto the electrode surface (Fig. 2B), observing a nearly 1.6-fold increase in the photocurrent response compared with that of pure CdS QDs, due to the possible fact that MB was served as an enhancer for high-efficiency increasing the photocurrent of CdS (Long et al., 2019). However, once numerous transformational Fc-DNAs generated from miRNA-224-induced 3D DNA walker amplification with the help of free-label DNA were modified onto the surface of ITO/CdS/MB-DNA electrode, a dramatically decreased photocurrent was observed, due to the "Y"-shaped ternary conjugate triggering the approach of quencher Fc and the departure of sensitizer MB to CdS, the photocurrent significantly decreased to ~47.06 μA (Fig. 2C) (Zhu et al., 2019). Furthermore, the transformational Fc-DNA and Ag-DNA were assembled on the same ITO/CdS/MB-DNA electrode surface, the photocurrent further decreased (29.18 μA, Fig. 2D), due to except the approach of quencher Fc and the departure of sensitizer MB toward CdS, the energy transfer between CdS and Ag could effectively weaken the PEC response (Zhu et al., 2019; Ma et al., 2016). These results indicate that the multiple signal amplification effect of substrate CdS is suitable for constructing the PEC biosensor for highly sensitive detection of miRNA-224.

Also, to understand the PEC signal quenching and enhancing on substrate CdS, the possible photocurrent generating mechanism was discussed. As described in Fig. 2F, under excitation light source, for CdS/MB sensitized structure, electrons of CdS transferred from VB to CB, and electrons of MB transferred to LUMO from HOMO, respectively. Afterward, the photo-generated electrons on LUMO of MB migrated to the CB of CdS and then moved to the bare ITO electrode, thus achieving an enhanced photocurrent response (Zhu et al., 2019). At the same time, AA was served as electron donor to promote charge separation and restrain the recombination of electron/hole pairs, so acquiring a strong photocurrent. Unfortunately, for CdS/Fc/Ag structure (Fig. 2G), parts of the photo-generated electrons on the CB of CdS competitively transferred to the LUMO of Fc, resulting in reduced electrons on the CB of CdS move to the bare ITO electrode (Zhu et al., 2019). In addition, the plasmon band of Ag NCs possessed great overlap with that of CdS QDs, which made possible an energy transfer process between the CdS QDs and Ag NCs, leading to a further decreased photocurrent (Ma et al., 2016).

On the other hand, a SWV characterization was performed to affirm the feasibility of the developed EC biosensor. From Fig. 2H, in the absence of miRNA-224, the EC signals were negligible because of the non electrochemical activity of CdS (curve a), which only acted as a

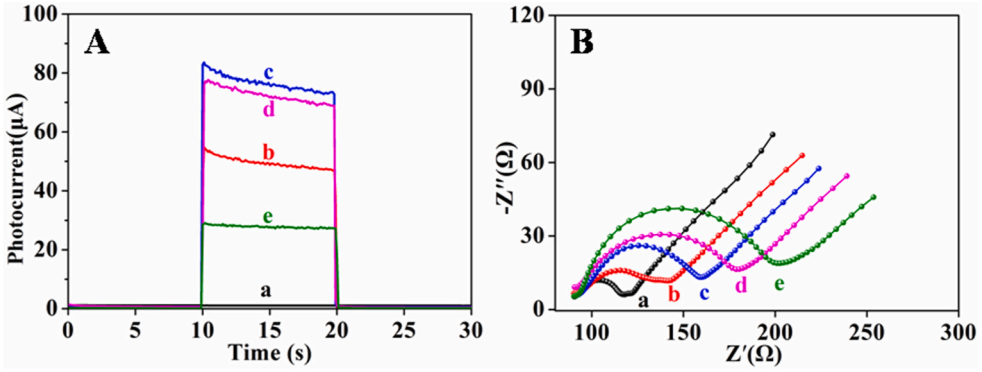

Fig. 3. (A) Photocurrent responses and (B) EIS results of the different electrodes (a) ITO, (b) ITO/CdS, (c) ITO/CdS/MB-DNA, (d) ITO/CdS/MB-DNA/MCH, (e) ITO/CdS/MB-DNA/MCH electrode after incubation with transformational Fc-DNA and Ag-DNA.

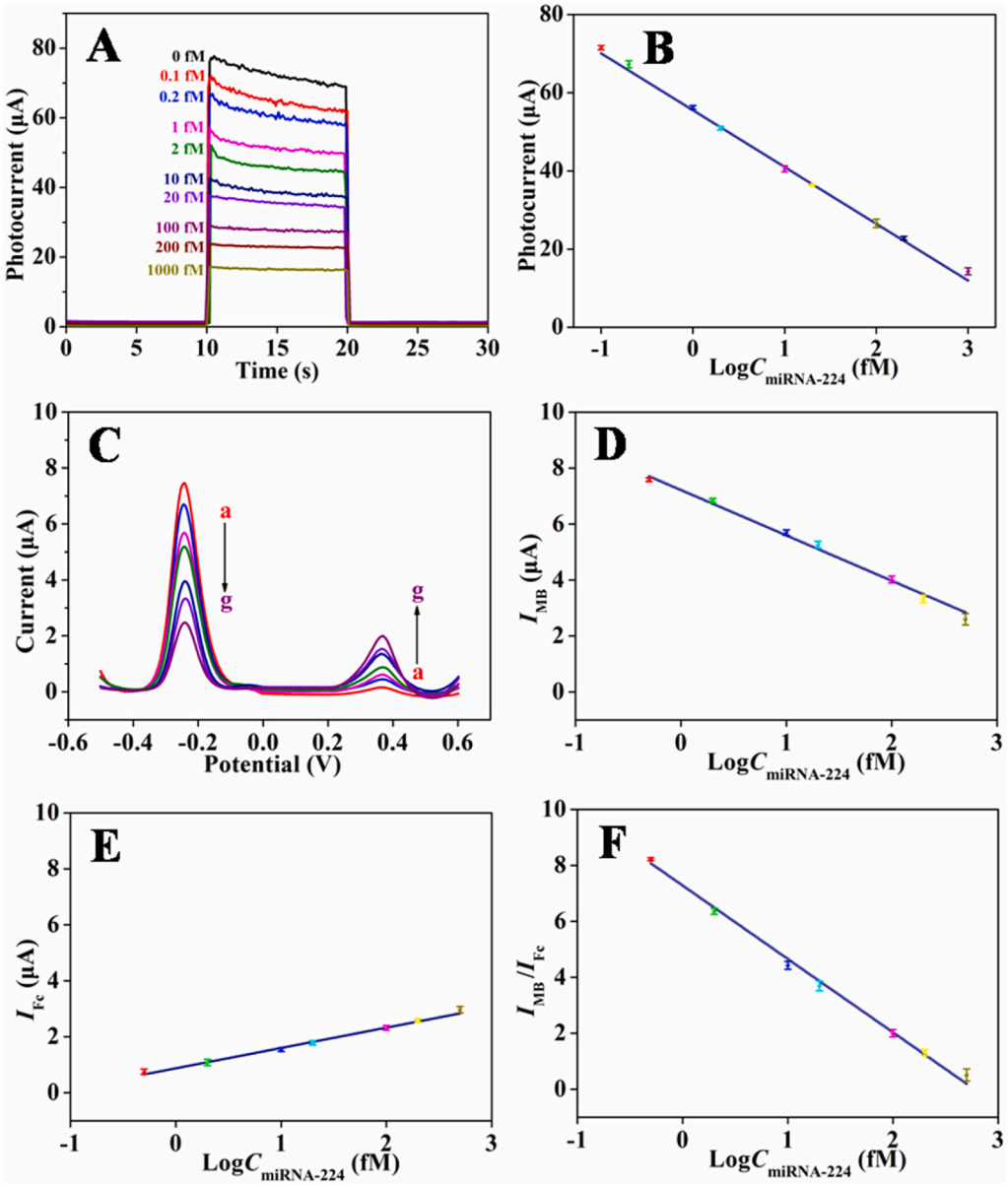

Fig. 4. (A) Photocurrent signals of the proposed PEC biosensor for miRNA-224 concentration from (a) to (i): 0.1, 0.2, 1, 2, 10, 20, 100, 200 and 1000 fM. (B) The corresponding linear curve. (C) SWV responses of the proposed EC biosensor for miRNA-224 concentration from (a) to (g): 0.5, 2, 10, 20, 100, 200, and 500 fM. Dependence of (D) I_{MB}, (E) I_{Fc}, (F) I_{MB}/I_{Fc} on the logarithm of miRNA-224 concentration. Three independent experiments for the average and standard deviation.

carrier to improve the modified electrode surface area. After stepwise modifying with MB-DNA, a remarkable oxidation peak of MB at about −0.25 V was received because of its high-efficiency electron transfer (curve b) (Zhu et al., 2018). However, when the modified electrode was incubated with miRNA-224-induced Fc-DNA and Ag-DNA (curve c), an outstanding oxidation peak of Fc (about 0.35 V) and a decreased that of MB were achieved (Xiong et al., 2017). Based on these results from Fig. 2 and Fig. S2, it is noted that the developed dual-model "on-super off" PEC/dual-signaling EC ratiometric biosensor can be adopted for miRNA-224 assay.

3.3. Fabrication characterization of the dual-model biosensor

To investigate the fabrication process of the biosensor, the PEC responses of the stepwise-modified procedure were carried out (Fig. 3A). After CdS QDs coated on the bare ITO electrode (curve a), a significantly enhanced photocurrent response was observed (curve b), because of the outstanding photoelectric property of CdS QDs. When MB-DNA is assembled onto the modified electrode surface, the photocurrent response further increased (curve c). Usually, the introduction of DNA sequences onto the surface of electrode would weaken the photocurrent (Wen and Ju, 2016; Zang et al., 2016). The wondrous enhanced result should be contributed to the dye-sensization effect of MB toward CdS (Zhu et al., 2019; Ma et al., 2016). The followed modification with MCH led to a decreased photocurrent (curve d). However, the photocurrent decreased dramatically after the ITO/CdS/MB-DNA1/MCH electrode subjecting to the mixture of transformational Fc-DNA and Ag-DNA (curve e), which was attributed to the dramatical quenching effect of Fc, the weak sensization effect of MB and energy transfer effect between CdS QDs and Ag NCs.

Simultaneously, EIS was investigated to further evidence stepwise assembly of the dual-model biosensor. From Fig. 3B, the bare ITO electrode exhibited a small semicircle diameter (curve a) because of the fast charge-transfer process (R_{ct}). After the modification with semiconductor CdS QDs, the R_{ct} value increased (curve b). Then, the R_{ct} value successively increased with the in turn modification of negatively-

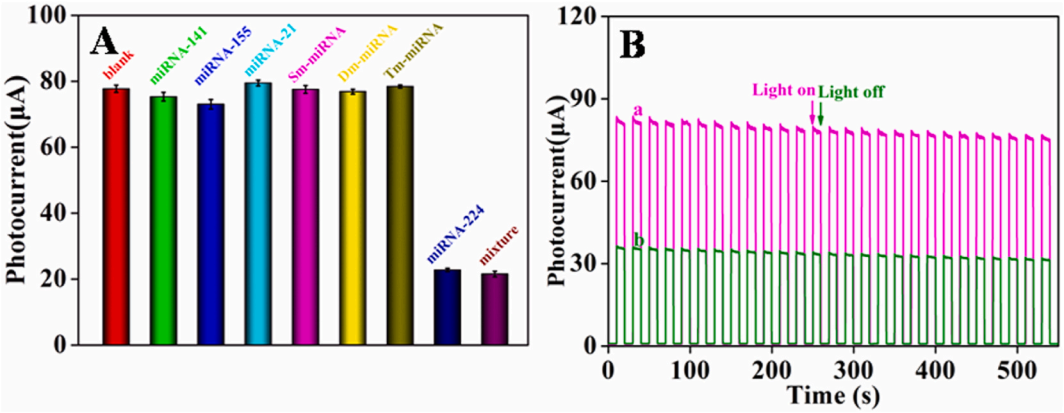

Fig. 5. Photocurrent responses of (A) the fabricated biosensor toward miRNA-224 (100 fM) and various interferences (5000 fM) and (B) the biosensing platform with continuous 27 cycles for (a) ITO/CdS/MB-DNA electrode (b) ITO/CdS/MB-DNA/MCH/Fc-DNA + Ag-DNA electrode toward 20 fM miRNA-224. Three independent experiments for the average and standard deviation.

charged DNA (curve c) and poor-conductive MCH (curve d). When the obtained electrode was reacted with intermediated Fc-DNA and Ag-DNA, the hybridization was performed in MB-DNA, Fc-DNA and Ag-DNA, resulting in an enhanced R_{ct} value (curve e), indicating the successful formation of the "Y"-shaped conformation. The obtained results indicate the successful preparation of dual-model biosensor for miRNA-224 detection (Scheme 1).

3.4. Dual-model biosensor for miRNA-224 detection

To investigate analysis capability of the proposed dual-model biosensor, PEC responses were first carried out toward a series of miRNA-224 concentrations under optimal experimental conditions (Figs. S3A–B). From Fig. 4A, the photocurrent responses decreased with the increased concentrations of miRNA-224 from 0.1 to 1000 fM. Fig. 4B illustrated the corresponding linear response curve between the values of photocurrent responses and the logarithm of miRNA-224 concentrations. The linear regression equation was $I = -14.5231 \log C_{\text{miRNA-224}} + 55.5461$ ($R^2 = 0.9941$), and a detection limit of 0.019 fM (3σ) was calculated.

Meanwhile, a dual-signaling electrochemical ratiometric biosensor was investigated by SWV measurements. From Fig. 4C, the oxidation peak current of MB decreased and that of Fc increased with miRNA-224 concentrations increasing from 0.5 to 500 fM. The calibration curves of the EC biosensing system through individual MB or Fc as signal for miRNA-224 assay were illustrated in Fig. 4D and E. Both of them exhibited a satisfactory linear relationship between the logarithm of miRNA-224 concentrations from 0.5 to 500 fM and the SWV responses, with detection limit of 0.14 (MB signal, $R^2 = 0.9901$) and 0.23 fM (Fc signal, $R^2 = 0.9900$), respectively. Moreover, Fig. 4F revealed the calibration plot of the EC ratiometric detection of miRNA-224 by dependence of I_{MB}/I_{Fc} on the logarithm of miRNA-224 concentrations, and a linear regression equation was $I_{MB}/I_{Fc} = -2.6255 \log C_{\text{miRNA-224}} + 7.2839$, ($R^2 = 0.9982$) with a detection limit of 0.061 fM (3σ). It was noted that the limit of detection "I_{MB}/I_{Fc}" used as signal was much lower than that of I_{MB} or I_{Fc}.

Additionally, to our best knowledge, the detection limit of our proposed dual-mode biosensor is much lower than that of most other biosensors for miRNAs detection reported previously (Table S2), which indicates that the established biosensor has an improved sensitivity due to the 3D DNA walker circular amplification strategy and the distance-controllable signal enhancing and quenching.

3.5. Selectivity and stability of the proposed biosensor

To evaluate the selectivity of the fabricated biosensing platform for miRNA-224 detection, some interferences miRNAs including miRNA-21, miRNA-141, miRNA-155, single-base mismatched miRNA-224 (Sm-miRNA-224), double-base mismatched miRNA-224 (Dm-miRNA-224), three-base mismatched miRNA-224 (Tm-miRNA-224), and the mixture were employed as models. As illustrated in Fig. 5A, compared with the blank solution, no obvious change of photocurrent responses could be observed after the biosensor incubated with the interferences miRNAs. However, the photocurrent for miRNA-155 seemed like similar to 0.1 fM of miRNA-224. Six additional experiments were made carefully for them to distinguish the photocurrents, respectively. As shown in Table S3, statistical significance analysis of them was characterized by using a *t*-test method (Qiu et al., 2018; Ding et al., 2020), and the photocurrent responses for miRNA-155 were higher than those from 0.1 fM of miRNA-224 ($t = 5.777$, $P < 0.001$), demonstrating that the developed biosensor could clearly distinguish the photocurrents between miRNA-155 and 0.1 fM of miRNA-224. On the contrary, the photocurrent response showed significant decrease in the present of target miRNA-224 or mixture, revealing the superior selectivity of the designed biosensing strategy.

The stability of the developed sensor was also characterized. From Fig. 5B, it was clear that the photocurrent responses of ITO/CdS/MB-DNA electrode (curve a) or ITO/CdS/MB-DNA/MCH/Fc-DNA + Ag-DNA electrode corresponding to 20 fM miRNA-224 (curve b) after consecutive 27 cycles with "off-on-off" light illumination exhibited negligible changes, respectively. On the other hand, the storing stability of the biosensor was investigated by at 4 °C in refrigerator with 15 days, the photocurrent of the responses could maintain about 96.4% of its initial photocurrent toward miRNA-224. The results reveal that the biosensing platform possesses satisfactory stability.

3.6. Recovery test

To evaluate the feasibility and application potential of the developed biosensing platform in complex biological system, the standard addition method was performed by PEC characterization to supervise miRNA-224 levels in a real human serum sample (collected from the First Affiliated Hospital of Zhengzhou University, China). The real sample was diluted to 10−fold by 10 mM PBS (pH 7.4) and poured in 0.1, 1, 10, 100, and 1000 fM miRNA-224 standards. Table S4 showed the obtained average and standard deviation of found photocurrents or concentrations ($n = 3$). The recoveries of the added miRNA-224 were 101.3%, 105.3%, 106.5%, 97.5% and 96.6%, respectively. The above results suggest that the proposed biosensor has potential application in miRNA-224 assay in actual sample monitoring.

4. Conclusions

Based on biofunctionalized nanostructures-driven signal enhancing and quenching strategies combined with 3D DNA walker strategy, a dual-mode "on-super off" PEC/ratiometric EC biosensor was successfully designed for the reliable and ultrasensitive detection of miRNA-224. Firstly, the MB-DNA sensitized CdS QDs as superior substrate exhibited outstanding photoelectric performance. Then the introduction of target-induced 3D DNA walker producing Fc-DNA and Ag-DNA resulted in a significantly decreased photocurrent response, due to the sensitizer MB diffuse away from the ITO electrode while the quencher Fc affixed close to it, accompanying with energy transfer process both CdS QDs and Ag NCs. As a result, miRNA-224 could be detected based on the dual-signaling EC ratiometric method for complementary PEC detection. Benefiting from different mechanisms and relatively independent signal transduction, the developed dual-mode biosensor possessed high sensitivity, good selectivity, satisfactory stability, and great practical applications in bioanalysis and early disease diagnosis.

Credit authorship contribution statement

Ruiying Yang: Methodology, Investigation, Formal analysis, Writing-original draft, Funding acquisition, Project administration. **Guihua Jiang:** Investigation, Formal analysis, Validation. **Huimin Liu:** Conceptualization, Investigation. **Leiliang He:** Conceptualization. **Fei Yu:** Methodology. **Li'e Liu:** Conceptualization. **Lingbo Qu:** Resources. **Yongjun Wu:** Writing-review & editing, Supervision.

Declaration of competing interest

The authors declare that they have no known competing financial interests or personal relationships that could have appeared to influence the work reported in this paper.

Acknowledgements

This work was financially supported by China Postdoctoral Science Foundation (No. 2020M672259).

Appendix A. Supplementary data

Supplementary data to this article can be found online at https://doi.org/10.1016/j.bios.2021.113337.

References

Cao, W.H., Gao, W., Liu, Z.H., Hao, W.J., Li, X., Sun, Y.H., Tong, L.L., Tang, B., 2018. Anal. Chem. 90, 9125–9131.
Cheng, H., Li, W., Duan, S.D., Peng, J.X., Liu, J.Q., Ma, W.J., Wang, H.Z., He, X.X., Wang, K.M., 2019. Anal. Chem. 91, 10672–10678.
Deng, H.M., Chai, Y.Q., Yuan, R., Yuan, Y.L., 2020. Anal. Chem. 92, 8364–8370.
Dong, H.F., Zhang, J., Ju, H.X., Lu, H.T., Wang, S.Y., Jin, S., Hao, K.H., Du, H.W., Zhang, X.J., 2018. Anal. Chem. 84, 4587–4593.
Ding, L.H., Wu, Y.J., Duan, Y.J., Yu, S.C., Yu, F., Wang, J., Tian, Y.M., Gao, Z.B., Wan, Z. Z., He, L.H., 2020. ACS Sens. 5, 440–446.
Gai, P.P., Gu, C.C., Li, H.Y., Sun, X.Z., Li, F., 2017. Anal. Chem. 89, 12293–12298.
Gao, H., Zhang, J.F., Liu, Y., Tu, W.W., Wei, T.X., Dai, Z.H., 2019. Anal. Chem. 91, 12038–12045.
Gao, C.M., Yu, H.H., Zhang, L.N., Zhao, Y.H., Xie, J.X., Li, C.J., Cui, K., Yu, J.H., 2020. Anal. Chem. 92, 2902–2906.
Ge, J.J., Zhao, Y., Gao, X.S., Li, H.K., Jie, G.F., 2019. Anal. Chem. 91, 14117–14124.
Gu, Y., Song, J., Li, M.X., Zhang, T.T., Zhao, W.W., Xu, J.J., Liu, M.L., Chen, H.Y., 2017. Anal. Chem. 89, 10585–10591.
Kong, Q.K., Cui, K., Zhang, L.N., Wang, Y.H., Sun, J.L., Ge, S.G., Zhang, Y., Yu, J.H., 2018. Anal. Chem. 90, 11297–11304.
Li, P.X., Wei, M., Zhang, F., Su, J., Wei, W., Zhang, Y.J., Liu, S.Q., 2018. ACS Appl. Mater. Interfaces 10, 43405–43410.
Li, L., Zhang, Y., Ge, S.G., Zhang, L.N., Cui, K., Zhao, P.N., Yan, M., Yu, J.H., 2019a. Anal. Chem. 91, 10273–10281.
Li, Y.R., Chang, Y.Y., Ma, J., Wu, Z.Y., Yuan, R., Chai, Y.Q., 2019b. Anal. Chem. 91, 6127–6133.
Li, J., Weng, X., Mo, F., Han, M., Li, H.B., 2020a. Anal. Chem. 92, 15145–15151.
Li, L., Zhang, Y., Yan, Z., Chen, M.Q., Zhang, L.N., Zhao, P.N., Yu, J.H., 2020b. ACS Sens. 5, 1482–1490.
Li, H.B., Han, M., Weng, X., Zhang, Y.Y., Li, J., 2021. ACS Nano 15, 1710–1717.
Lv, S.Z., Zhang, K.Y., Zhu, L., Tang, D.P., 2020. Anal. Chem. 92, 1470–1476.
Long, D., Li, M.J., Wang, H.H., Wang, H.J., Chai, Y.Q., Yuan, R., 2019. Biosens. Bioelectron. 142, 111579.
Ma, Z.Y., Xu, F., Qin, Y., Zhao, W.W., Xu, J.J., Chen, H.Y., 2016. Anal. Chem. 88, 4183–4187.
Qiu, Z.L., Shu, J., Tang, D.P., 2018. Anal. Chem. 90, 12214–12220.
Tao, A., Sinsermsuksakul, P., Yang, P.D., 2006. Angew. Chem. Int. Ed. 45, 4597–4601.
Wen, G.M., Ju, H.X., 2016. Anal. Chem. 88, 8339–8345.
Xiong, E.H., Li, Z.Z., Zhang, X.H., Zhou, J.W., Yan, X.X., Liu, Y.Q., Chen, J.H., 2017. Anal. Chem. 89, 8830–8835.
Xue, H.H., Shen, W.J., Geng, W.C., Yin, X., Yang, Y., Guo, S.J., Li, Y.J., 2018. Chem. Commun. 54, 7227–7230.
Xu, M.D., Zhuang, J.Y., Jiang, X.Y., Liu, X.Z., Tang, D.P., 2019. Chem. Commun. 55, 9857–9860.
Yang, R.Y., Zou, K., Li, Y.M., Meng, L.X., Zhang, X.H., Chen, J.H., 2018. Anal. Chem. 90, 9480–9486.
Yang, R.Y., Zou, K., Zhang, X.H., Du, C.C., Chen, J.H., 2019a. Biosens. Bioelectron. 132, 55–61.
Yang, R.Y., Zou, K., Zhang, X.H., Du, C.C., Chen, J.H., 2019b. Chem. Commun. 55, 8939–8942.
Ye, J., Liu, G.Y., Yan, M.X., Zhu, Q.J., Zhu, L.P., Huang, J.S., Yang, X.R., 2019. Anal. Chem. 91, 13237–13243.
Zang, Y., Lei, J.P., Hao, Q., Ju, H.X., 2016. Biosens. Bioelectron. 77, 557–564.
Zhang, P.H., Wang, C., Zhao, J.J., Xiao, A.Q., Shen, Q., Li, L.T., Li, J.X., Zhang, J.F., Min, Q.H., Chen, J.N., Chen, H.Y., Zhu, J.J., 2016. ACS Nano 10, 3637–3647.
Zhang, K., Dong, H.F., Dai, W.H., Meng, X.D., Lu, H.T., Wu, T.T., Zhang, X.J., 2017. Anal. Chem. 89, 648–655.
Zhang, P., Jiang, J., Yuan, R., Zhuo, Y., Chai, Y.Q., 2018a. J. Am. Chem. Soc. 140, 9361–9364.
Zhang, Y., Shuai, Z.H., Zhou, H., Luo, Z.M., Liu, B., Zhang, Y.N., Zhang, L., Chen, S.F., Chao, J., Weng, L.X., Fan, Q.L., Fan, C.H., Huang, W., Wang, L.H., 2018b. J. Am. Chem. Soc. 140, 3988–3993.
Zhu, C.X., Liu, M.Y., Li, X.Y., Zhang, X.H., Chen, J.H., 2018. Chem. Commun. 54, 10359–10362.
Zhu, M.H., Zhong, X., Deng, H.M., Huang, L.J., Yuan, R., Yuan, Y.L., 2019. Biosens. Bioelectron. 143, 111618.